Multi-objective optimization algorithm for improving the efficiency of speeded up robust features of image stitching

Kittisak Sanprasit [a,1], Uraiwan Butsathip [b,2], Khomyuth Chaiwong [b,3,*]

[a] Faculty of Industrial Technology, Loei Rajabhat University, Loei, Thailand
[b] Faculty of Management Science, Loei Rajabhat University, Loei, Thailand
[1] kittisak.san@lru.ac.th; [2] uraiwan.but@lru.ac.th; [3] khomyuth.cha@lru.ac.th
* corresponding author

ARTICLE INFO

Article history
Received May 2, 2025
Revised July 2, 2025
Accepted July 2, 2025
Published November 30, 2025

Keywords
Stitching
MOWOA
MOGWO
MOGA
SURF

ABSTRACT

Image stitching to generate panoramic or composite images. This research proposes improved parameters for the fundamental matrix in the standard SURF method via multi-objective optimization. This paper compares three metaheuristic algorithms (MOWOA, MOGWO, MOGA) and evaluates their performance using the hypervolume indicator (HV). The optimal points were selected from non-dominated solutions using the MCDM and the weighted-sum method (WSM). There were two objective functions: 1) minimum of image subtraction and 2) minimum of histogram. The MOWOA is superior to the other. This approach significantly reduces stitching errors and improves performance by 24.48% over standard SURF. The proposed multi-objective optimization of fundamental matrix parameters significantly enhances SURF-based image stitching by reducing alignment and blending errors, resulting in smoother, more coherent panoramic or composite images. This is achieved by leveraging superior metaheuristic performance, particularly from MOWOA, which outperforms other algorithms. This approach increases stitching robustness and accuracy, making it highly valuable for real-world applications such as mapping, surveillance, and visual reconstruction.

1. Introduction

The main goal of image stitching or photo stitching is to combine two photographic images to produce a segmented panorama or high-resolution image. Image stitching is image registration, which means identifying overlapping areas of the image to be spliced and then determining the transformation relationship [1], [2]. These points are detected using two techniques: manual and automatic. The manual point-selection technique introduces errors when applied to multiple images or videos. On the other hand, the automatic technique outperforms the manual technique [3]. There are several automatic image feature extraction methods, for example, Harris [4], features from accelerated segment test (FAST) [5], scale invariant feature transform (SIFT) [6]–[8], speed-up robust features (SURF) [9]–[15] and compared with the SIFT and SURF feature extraction algorithms [1], [16], [17], have been fundamental research topics in the field.

Hao et al. [18] propose a robust stitching algorithm for fisheye images by combining traditional image processing techniques with deep learning. Saleem [19] presents a new MLESAC-based estimator that is compared with RANSAC for estimating the fundamental matrix to define the epipolar geometry for image stitching. Mo et al. [20] present a stitching method on Deep Feature in hyperspectral images (HSIs) captured by UAV. Lin et al. [21] proposed an automatic method that incorporates DBSCAN for

clustering 3D point cloud maps, which is essential for navigation and localization in Autonomous Mobile Robots. Wu et al. [22] used image Stitching for Soil organic matter (SOM). In other previous studies, image stitching often requires complex mathematical models. The estimation of the fundamental matrix in the standard SURF method using the Random Sample Consensus (RANSAC) technique. The results of generating panoramic or composite images are not smooth, which is an interesting topic in this research.

This paper presents improved parameters of the fundamental matrix in the standard SURF method using a meta-heuristic algorithm [23], [24] which is a popular technique because of its simplicity. This work also proposes a multi-objective optimization [25], [26] to reduce the difference and continuity between the original image and the generated panoramic or composite images. Two objective functions were employed: minimum image subtraction for analyzing image-stitching differences and the minimum histogram for evaluating image continuity, excluding noise sources such as image size, resolution, and illumination in this experiment. We compared multi-objective metaheuristics (MOMHs) [27] for the optimal design of the fundamental matrix parameters in the standard SURF method. The optimizers used three algorithms: Multi-objective Whale Optimization Algorithm (MOWOA) [25], [28]–[35], Multi-objective Grey Wolf Optimizer (MOGWO) [36]–[41], and Multi-Objective Genetic Algorithm (MOGA) [42]–[49]. The program was developed in MATLAB. The non-dominated solution was used to find the Pareto front. The performance of various optimizers was compared using the hypervolume (HV) indicator [27]. The minimal weighted sum (MWS) method was used to select the optimal point on the Pareto front. Therefore, this research aims to enhance SURF's stitching efficiency using multi-objective optimization techniques. This paper compares three metaheuristic algorithms (MOWOA, MOGWO, MOGA) and evaluates their performance using the hypervolume indicator and WSM.

This paper begins with an introduction, followed by the method, which includes image stitching, and the numerical simulation is explained in Section 2. The experimental results and discussion are shown in Section 3. Finally, the conclusion is made in Section 4.

2. Method

2.1. Image Stitching

In this section, we describe how to stitch two or more images into a single larger image, as shown in Fig. 1. Feature-based image stitching technology is widely used because it offers high time efficiency, maximum matching accuracy, and good robustness [1].

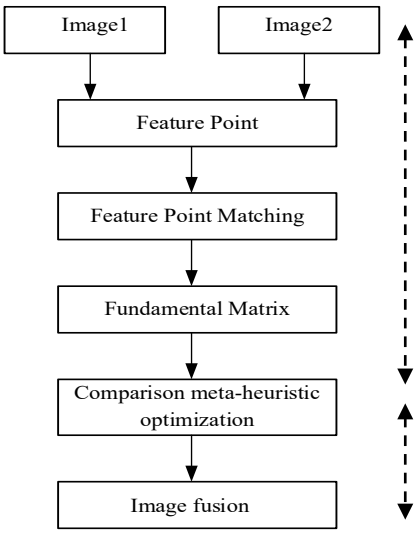

Fig. 1. The process of image panoramic

This paper stitches two images using the Speeded Up Robust Features (SURF) method. It can be divided into four steps: feature point extraction, feature point matching, determination of the transformation relationship, and image fusion. The purpose of modifying the fundamental matrix is to define the epipolar geometry by an optimization method. We compare multi-objective meta-heuristics for the optimum design of a basic matrix on SURF. The optimizers use three algorithms: MOWOA, MOGWO, and MOGA. The MOWOA and MOGWO algorithms are similar in that they mimic the natural behavior of animals. MOGA is a widely used algorithm for comparison with other algorithms. Three algorithms have not yet been applied to the analysis of panoramic images.

2.2. Transformation Relationship

Before image fusion, the relationship between two or more images with different transformations is called epipolar geometry. The relation that links the scenes with different modifications is named the fundamental matrix [3]. The initial transformation matrix or fundamental matrix [1]. The image transformation matrix has eight parameters; these parameters represent the picture of the scale variable, rotation, and horizontal and vertical displacement (which gives the details about the entire transformation of an image with eight unknowns); see (1) [50]. It is an iterative method to estimate parameters of a mathematical model by Random Sample Consensus (RANSAC) method is derived as in (1).

$$\begin{bmatrix} x' \\ y' \\ 1 \end{bmatrix} = \begin{bmatrix} h_1 & h_2 & h_3 \\ h_4 & h_5 & h_6 \\ h_7 & h_8 & 1 \end{bmatrix} \begin{bmatrix} x \\ y \\ 1 \end{bmatrix} \tag{1}$$

where $h_1,\ldots,h_8$ represent parameters of the transformation matrix. Given a point (x, y) in an image and a new point (x, y) after the multiplication by the transformation matrix, respectively.

2.3. Process and results of SURF

In this part, we use an image of Phu Ruea National Park, Loei Province, Thailand, for the image-stitching experiment using the standard Speeded-Up Robust Features (SURF) method. Image 1, as shown in Fig.2(a) has a resolution of 1,107 × 604 pixels in JPG format with a file size of 258 KB, while Image 2 (Fig. 2(c)) has a resolution of 767 × 754 pixels in JPG format with a file size of 197 KB. Before feature extraction, both images were converted to grayscale, as shown in Fig. 2(b) and Fig. 2(d).

(a) Image 1 (b) Image 1 in grey mode (c) Image 2 (d) Image 2 in grey mode

Fig. 2. The Phu Ruea National Park

In the next step, SURF key points were detected independently in both images the feature point for image 1 and image 2, as shown in Fig. 3. These keypoints were then matched based on descriptor similarity to establish point correspondences between the two images, as presented in Fig. 4. Finally, the parameters of the fundamental matrix in standard SURF were calculated by the RANSAC method, shown in Table 1, and moved image 2, as shown in Fig. 5. The results of generate panoramic or composite image is distorted, the sky lines are not aligned, and the letters cannot be combined.

Fig. 3. The feature points for Image 1 and Image 2

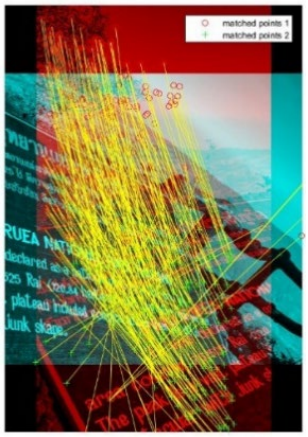

Fig. 4. The feature point matching for Image 1 and Image 2

To estimate the geometric relationship between the images, the fundamental (transformation) matrix was computed using the Random Sample Consensus (RANSAC) algorithm to eliminate outliers and retain robust matches. The resulting transformation matrix parameters obtained from the standard SURF approach are listed in Table 1.

Table 1. The Parameter of the Transformation Matrix of SURF

Parameter	value
h_1	0.8484
h_2	-0.4743
h_3	0
h_4	0.6741
h_5	0.7181
h_6	0
h_7	153.1096
h_8	468.2344

Based on this transformation, Image 2 was geometrically aligned and translated relative to Image 1, as shown in Fig. 5(a), and subsequently stitched to form a composite image (Fig. 5b).

(a) Move image 2

(b) Stitch image 2 to image 1

Fig. 5. Stitching two images by the SURF method

However, the final panoramic result exhibits noticeable distortions. Specifically, the skyline is misaligned, and the text regions do not merge seamlessly. These artifacts indicate that the standard SURF-based transformation, despite successful feature detection and matching, is insufficient to account for perspective variations and complex scene geometry in this dataset, resulting in suboptimal stitching quality.

2.3.1. Numerical Simulation

The numerical simulation presents a step-by-step procedure for implementing the proposed numerical simulation, which is outlined as follows:

Step 1: Define the epipolar geometry to relate two 2D images.

Step 2: Determining the fundamental matrix by the Speeded-Up Robust Features (SURF) technique.

Step 3: Calculate two objective functions.

Step 4: Process of meta-heuristic optimization Algorithm of Multi-objective by MOWOA, MOGWO, and MOGA techniques.

Step 5: The performance comparison meta-heuristic optimization based on the hypervolume (HV)

Step 6: Select the best Pareto archive from the best optimization algorithm of Multi-objective using the weighted sum method (WSM).

Step 7: Return the best of the Pareto archive and the designed variables for experiments in image stitching.

2.3.1.1. Multi-objective of image stitching

Multi-objective optimization is a design approach for determining the optimal point. For a problem with more than one objective function, there is more than one optimal solution. The traditional combination of these results is called a set of Pareto-optimal solutions, or a Pareto front, viewed in the objective-function domain. A typical mathematical formulation of multi-objective optimization is given in (2).

$$Minimize: F(x) = \{f_1(x), f_2(x), \dots, f_o(x)\} \tag{2}$$

constraint to:

$$\begin{aligned} &g_i(x) \leq 0, i = 1, \dots, m \\ &h_i(x) = 0, i = 1, \dots, m \\ &L_i \leq x_i \leq U_i, i = 1, \dots, n \end{aligned} \tag{3}$$

where x and f_i represent the design variable and objective functions, respectively. $f_o(x)$ represents the objective functions. Function $g_i(x)$ and $h_i(x)$ are the inequality and equality constraints, while L_i and U_i are lower and upper bound constraints. Parameters m, i and n are a number of variables and o is the number of objective functions.

2.3.1.2. Objective functions

The designed parameter of the transformation matrix for solving the problem in this study. The designed variable of 8 parameter $(h_1, \dots, h_8)$ and h_3, h_6 is 0 value all time, see (4). There are two objective functions: the minimum image subtraction to reduce the difference between the original image and the generated panoramic or composite images, and the minimum histogram for continuity between the original image and the generated panoramic or composite images, without noise such as image size, resolution, light, etc., for this experiment. However, in the future, there may be further experiments in the case of indoor, aerial, and distorted image differences. Details can be described as follows.

$$x = [h_1\, h_2 \dots h_8] \tag{4}$$

- Minimum of image subtraction. The difference image is an image processing technique that results in image subtraction from a calculated value of grayscale in the original image, subtracted from the value of grayscale in the generated panoramic images, and the objective function presented in.

$$f_1 = min \sum_{p=1}^{p=max\Sigma} (|f(x,y) - h(x,y)|) \quad (5)$$

when $f_1, f(x,y), h(x,y)$ represent the first objective function; the grayscale values in the original image and in the generated panoramic images have a resolution of 1,107x604 pixels, corresponding to 668,628 positions, respectively.

- Minimum of histogram. In this work, the difference histogram is a technique for evaluating the continuity of an image and a popular method for image contrast enhancement, and the objective function is presented in (6).

$$f_2 = min \sum_{g=0}^{g=1} (|f_{Pixes}(x,y) - h_{Pixels}(x,y|) \quad (6)$$

when $f_2, f_{Pixes}(x,y), h_{Pixels}(x,y)$ represent the second objective function, the value of grayscale in the original image, and the value of grayscale (0-1) in generated panoramic images.

2.3.1.3. Numerical experiment

This investigation is conducted using MATLAB software, and the setup is shown in section 3.1. For each test system, 4 independent runs for each optimizer were operated, and a comparative study of multi-objective meta-heuristics (MOMHs) for optimum design of image stitching.

2.3.1.4. Non-Dominated solutions

To solve multi-objective problems, the non-dominated solutions are identified, and the Pareto archive is employed. The step-by-step procedure for the implementation of the proposed algorithm is outlined below [27]:

Step 1: Initialize the population of the design variable vector of the transformation relationship by the RANSAC method, shown in Table 1. The designed variable of 8 parameters ($h_1,...,h_8$) and h_3, h_6 is 0 value all the time.

$$H = \begin{bmatrix} h_1 \\ h_2 \\ \vdots \\ h_n \end{bmatrix} \begin{bmatrix} h_{1,1} & \cdots & h_{1,8} \\ h_{2,1} & \cdots & h_{2,8} \\ \vdots & \cdots & \vdots \\ h_{n,1} & \cdots & h_{n,8} \end{bmatrix} \quad (7)$$

when $h_1 - h_2, h_4 - h_6$ are the values range ± 0.1, h_7, h_8 are the values range ± 5 and h_3, h_6 are 0. The subscript n is the population size or number of search agents.

Step 2: Evaluate the fitness evaluation of a design variable vector. For the two objectives f_1, f_2 and the vector solution, F is a feasible solution in the inequality constraints.

$$F(Q) = \begin{bmatrix} f_1(h_1) & f_2(h_1) \\ f_1(h_2) & f_2(h_2) \\ \vdots & \vdots \\ f_1(h_2) & f_2(h_n) \end{bmatrix} \quad (8)$$

Step 3: Determine the non-dominated solution (NS) as shown in Fig. 6. They store and update a set of non-dominated solutions in the Pareto archive (P).

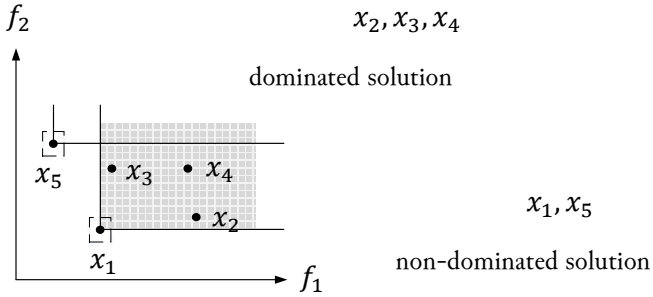

Fig. 6. Non-dominated solutions.

Step 4: Select the best solution from the Pareto archive using the roulette wheel technique and grid mechanism.

Step 5: Update the best solution. If there are better solutions, then the next generation is generated.

Step 6: Repeat steps 1 to 5 until a termination criterion is met.

2.3.1.5. Hypervolume

The hypervolume is the volume (for 3D) or area (for 2D) covered by non-dominated solutions and measured for a defined reference point (as shown in Fig. 7), which can be calculated as follows [27]:

$$HV = \sum_{i=1}^{n} Vi \quad (9)$$

where HV is hypervolume, V_i is the volume or area of a hypercube, that is created by the i^{th} non-dominated solution and reference point.

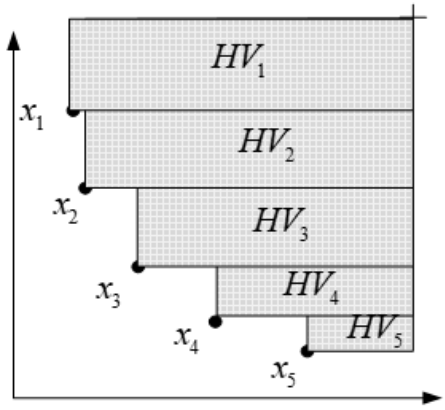

Fig. 7. Area to calculate HV

2.3.1.6. Multi-Criteria Decision Making (MCDM) methods

To select the best Pareto archive, the MCDM method and the weighted-sum method (WSM) are employed. The multi-criteria utility function is introduced (10) [27].

$$V = \sum_{i=1}^{k} w_i F_i(x) \quad (10)$$

where $U, w_i, F_i(x), i, k$ represent the multi-criteria utility function, the weight assigned, the objective function, the number of objective functions, and the maximum of the objective function, respectively. The objective functions may be converted to their normal forms as follows:

$$U = w_1 \left(\frac{f_1(x) - f_1^{min}}{f_1^{max} - f_1^{min}} \right) + w_1 \left(\frac{f_2(x) - f_2^{min}}{f_2^{max} - f_2^{min}} \right) \quad (11)$$

where $U, w_1, w_2, f_1(x), f_1^{max}, f_1^{min}, f_2(x), f_2^{max}, f_2^{min}$ represent the multi-criteria utility function, the weight assigned to the first objective, the weight assigned to the second objective, the first objective function, maximize of the first objective function, minimize of the first objective function, the second objective function, maximize of the second objective function, minimize of the second objective function, respectively.

3. Results and Discussion

As shown in the previous section, the simulation depicts the experiment's image stitching.

3.1. Parameter settings

The general parameters of various algorithms in MATLAB programming such as the population size or number of searchagents (na) = 30, number of population (npop) = 8, the maximum number of iteration (niter) = 500, size of Pareto archive (narchive) = 300, number of grid per each dimension (ngrid) = 10, reference point (rp)= 1.5 for the hypervolume, weight assigned to the first objective (w1) =0.5 and weight assigned to the second objective (w2) =0.5 for the weighted sum method (WSM), The other parameters used explicitly by a particular optimizer are given below:

- Multi-objective Whale Optimization Algorithm (MOWOA) setting: vector $\vec{\alpha}$ is linearly decreased from 2 to 0, a constant for defining the shape of the logarithmic spiral (b) = 1.
- Multi-objective Grey Wolf Optimizer (MOGWO) setting: grid inflation parameter (alpha) = 0.1, leader selection pressure parameter (beta) = 4, and extra (to be deleted) repository member selection pressure (gamma) = 2.
- Multi-objective Genetic Algorithm (MOGA) setting: crossing-over probability (pc) = 1.0, and mutation probability (pm) = 0.1.

3.2. Simulation result

The multi-objective functions optimized using the proposed MOWOA, MOGWO, and MOGA comparative algorithms are shown in Fig. 8. These figures illustrate the convergence of the Pareto archive. The performance compared based on the hypervolume (HV) is shown in Fig. 9.

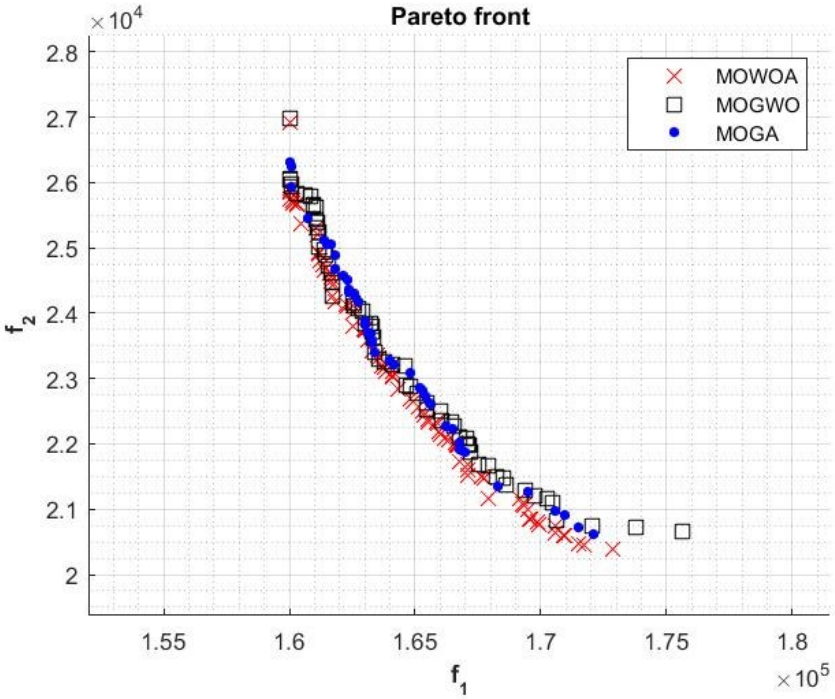

Fig. 8. Best Pareto front from each algorithm.

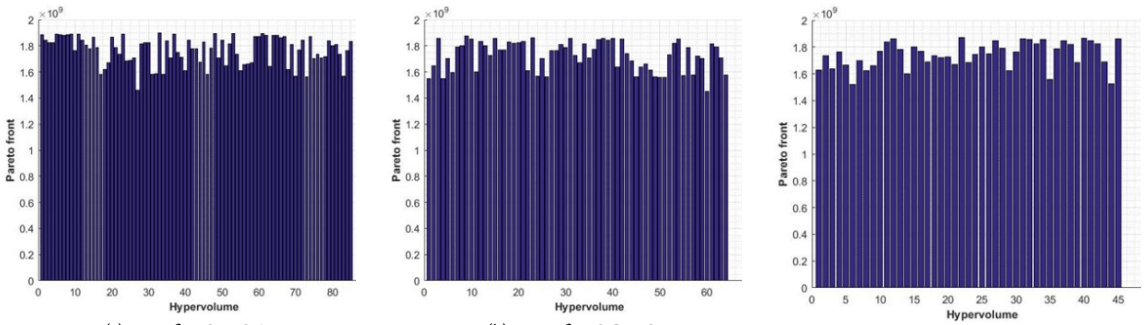

(a) HVof MOWOA (b) HV of MOGWO (c) HV of MOGA

Fig. 9. The Hyper volume (HV)

The reference point for calculating the hypervolume indicator is the maximum value for the better algorithm. Results obtained using algorithms MOWOA, MOGWO, and MOGA are reported in Table 2.

Table 2. Hypervolume values

Algorithm	Minimum	Maximum	Mean	Std. Dev.
MOWOA	1,458,207,777	1,897,539,801	1,766,737,837	108,028,649
MOGWO	1,451,559,487	1,875,012,573	1,725,584,802	111,617,408
MOGA	1,520,597,935	1,872,699,444	1,744,161,939	96,836,565

MOWOA outperforms the others, achieving a maximum of 1.2%; it is superior to the others. The best Pareto front of MOWOA obtained in this study is illustrated in Fig. 10, and the minimization weighted-sum method (11) yields 0.3563. The first objective function is 164,344 positions, and the second objective function is 22,846 pixels, as shown in Fig. 10. The designed variable is shown in Table 3.

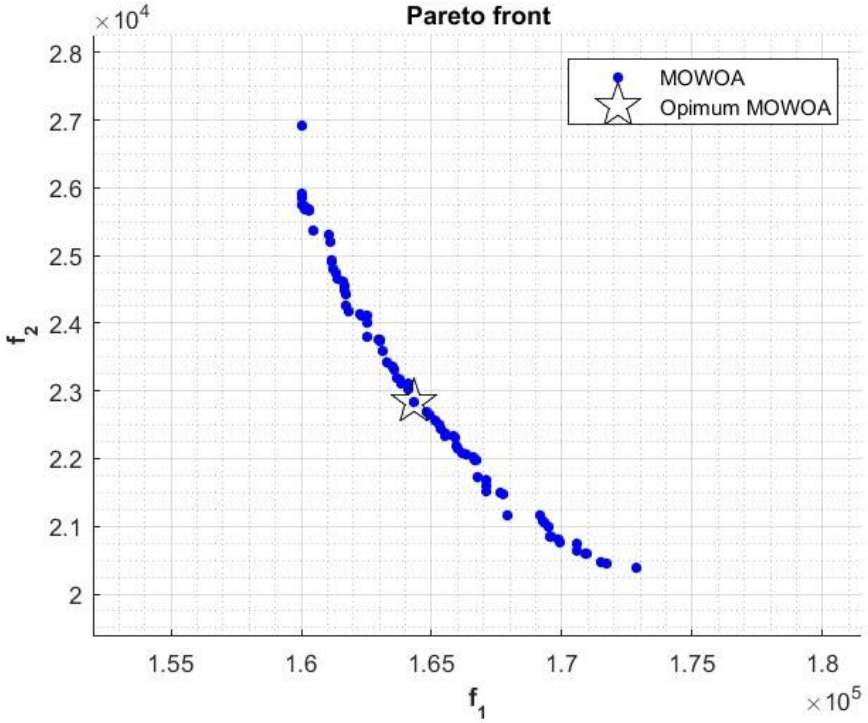

Fig. 10. The best-obtained Pareto front of MOWOA and the Optimum point.

The geometric transformation employed in the proposed MOWOA technique is defined by a set of eight parameters $(h_1–h_8)$, as summarized in Table 3. Parameters $h_1$to $h_6$represent the linear components of the transformation matrix, where the nonzero values indicate combined scaling and rotation effects, while the zero-valued coefficients (h_3 and h_6) suggest the absence of shear along the corresponding axes. Specifically, the symmetric values of $h_1 = h_5 = 0.8181$and the opposite signs of $h_2$and $h_4(-0.5743$ and 0.5741, respectively) reflect a rotation-dominant transformation with uniform scaling. The remaining parameters, $h_7 = 148.1096$and $h_8 = 472.8398$, correspond to translation components along the horizontal and vertical directions, respectively, enabling accurate spatial alignment during the transformation process. Collectively, these parameters define a stable and well-conditioned transformation matrix optimized by the MOWOA approach.

Table 3. The parameter of the transformation matrix of the MOWOA techniques

PARAMETER	VALUE
h_1	0.8181
h_2	-0.5743
h_3	0
h_4	0.5741
h_5	0.8181
h_6	0
h_7	148.1096
h_8	472.8398

3.3. Results and analysis

The analyzed image measures 1,107 x 604 pixels. The calculated minimum image subtraction for the experimental results, using the SURF method, is 215,566 positions, whereas the MOWOA value is 164,344 positions. The SURF histogram minimum is 30,548 pixels, and the MOWOA histogram minimum is 22,846 pixels, as presented in Table 4.

Table 4. The comparison result of the objective function

Experimental	SURF	MOWOA	Improvement
Minimum of image subtraction (position)	215,566	164,344	23.76%
Minimization of histogram (pixels)	30,548	22,846	25.21%

The results of MOWOA improved SURF for the first objective function by 23.76% and for the second objective function by 25.21%, resulting in an overall improvement of 24.48% over standard SURF. The experiments yield panoramic results for SURF and MOWOA, as shown in Fig. 11. The results produce panoramic (Fig. 11(b)) or composite images that are not distorted, with aligned skylines and letters that can be combined. The histogram image SURF and MOWOA, as shown in Fig. 12. However, this is an offline experiment, not a real-time experiment. Future experiments may include additional conditions (e.g., image size, resolution, illumination), or incorporate an objective function.

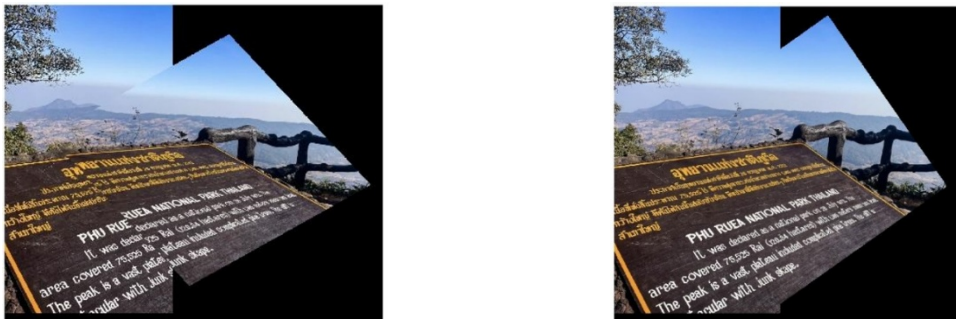

(a) SURF (b) WOWOA

Fig. 11. Comparison result of SURF and MOWOA techniques.

Fig. 12(c) illustrates the histogram-based error distribution between the SURF and MOWOA approaches across normalized gray levels [0,1]. The error exhibits pronounced peaks in the low–mid gray-level range (approximately 0.15–0.30), indicating regions where intensity discrepancies between the two methods are most significant. In contrast, the mid-range gray levels (≈0.35–0.70) show comparatively lower and more stable error values, suggesting improved consistency in feature alignment and intensity mapping. A secondary increase in error occurs at higher gray levels (≈0.75–0.85), followed by a sharp spike near the upper bound, which may be attributed to boundary effects or high-contrast regions. Overall, the distribution highlights non-uniform error behavior across intensity levels, reflecting the differing sensitivities of SURF and MOWOA to local intensity variations during stitching.

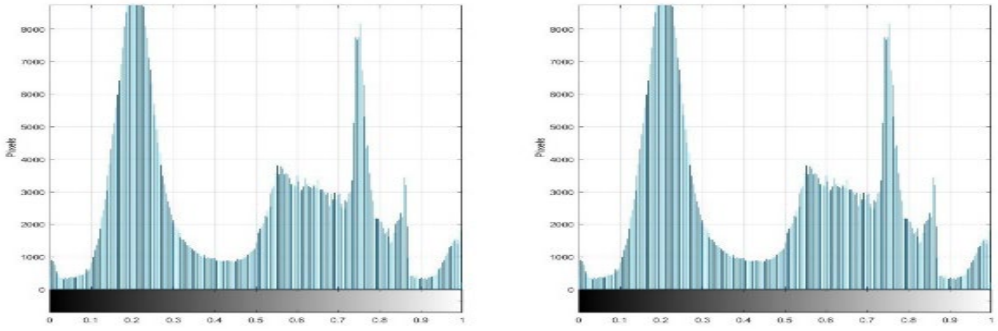

(a) SURF (b) MOWOA

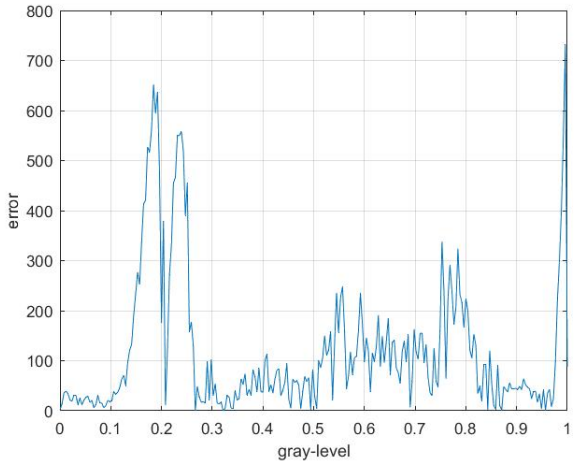

(c) Error of histogram between SURF and MOWOA

Fig. 12. The histogram

4. Conclusion

This paper proposes improved parameters of the fundamental matrix in the standard SURF method using a meta-heuristic algorithm. This paper compares three metaheuristic algorithms (MOWOA, MOGWO, MOGA) and evaluates their performance using the hypervolume indicator and WSM. First, we discussed the motivation for this research and explained why the proposed strategy is necessary. Second, we stitch two images using the Speeded Up Robust Features (SURF) method. The resulting image transformation matrix has eight parameters, which are estimated using the Random Sample Consensus (RANSAC) method. Third, we increase efficiency through metaheuristic multi-objective optimization algorithms, namely MOWOA, MOGWO, and MOGA. This work also proposes a comparative study of multi-objective meta-heuristics (MOMHs). Subsequently, the multi-objective test functions were optimized using the proposed MOWOA, MOGWO, and MOGA comparative algorithms. Performance was evaluated using the hypervolume (HV) indicator. MOWOA yields the best result. To select the best Pareto archive, the MCDM method and the minimization weighted sum method (WSM) are 0.3563. The first objective function (minimum of image subtraction) is 164,344

positions, and the second objective function (minimization of histogram) is 22,846 pixels. Finally, the results of the best Pareto archive of MOWOA are applied to the generated panoramic image. The experiments present results for 2 objective functions. 1) The minimum of image subtraction between the SURF method and the MOWOA result. The minimum image subtraction of the MOWOA result achieves a 23.76% improvement over the SURF method. 2) The minimization of the histogram, the MOWOA result achieves a 25.21% better result than the SURF method. In summary, MOWOA's optimization techniques improved the efficiency of the SURF method by 24.48%. However, in the future, the generated panoramic images will be used in mobile mapping, UAVs, and medical applications.

Declarations

Author contribution. Kittisak Sanprasit, Uraiwan Butsathip, and Khomyuth Chaiwong developed the theory, performed the computations, and performed the numerical simulations and experiments at the Department of Electrical and Electronic Engineering, Faculty of Industrial Technology, Loei Rajabhat University, Loei, Thailand.

Funding statement. The National Science, Research and Innovation Fund (NSRF) by the Research and Development Institute, Loei Rajabhat University.

Conflict of interest. The authors declare no conflict of interest.

Additional information. No additional information is available for this paper.

References

[1] M. V. Gowda, and G. Padmajadevi, "Image Stitching Using Speeded Up Robust Features," *Int. J. Recent Innov. Trends Comput. Commun.*, vol. 3, no. 6, pp. 3514–3519, Jun. 2015, doi: 10.17762/IJRITCC.V3I6.4483.

[2] J. Choi, H. Lim, S. Yun, M. Shin, and J. Paik, "Image Stitching Method for Surround View Image without Seamline," in *2023 International Conference on Electronics, Information, and Communication (ICEIC)*, Feb. 2023, pp. 1–3, doi: 10.1109/ICEIC57457.2023.10049955.

[3] A. Chater, H. Benradi, and A. Lasfar, "Method of optimization of the fundamental matrix by technique speeded up robust features application of different stress images," *Int. J. Electr. Comput. Eng.*, vol. 12, no. 2, p. 1429, Apr. 2022, doi: 10.11591/ijece.v12i2.pp1429-1436.

[4] H. Wang, M. M. Ullah, A. Klaser, I. Laptev, and C. Schmid, "Evaluation of local spatio-temporal features for action recognition," in *Procedings of the British Machine Vision Conference 2009*, 2009, pp. 124.1-124.11, doi: 10.5244/C.23.124.

[5] Q. Zhu, S. Avidan, M. C. Yeh, and K. T. Cheng, "Fast human detection using a cascade of histograms of oriented gradients," in *Proceedings of the IEEE Computer Society Conference on Computer Vision and Pattern Recognition*, 2006, vol. 2, pp. 1491–1498, doi: 10.1109/CVPR.2006.119.

[6] S. C. Manda, S. Muttineni, G. Venkatachalam, B. C. Kongara, and R. Senapati, "Image Stitching using RANSAC and Bayesian Refinement," in *2023 3rd International Conference on Intelligent Technologies (CONIT)*, Jun. 2023, pp. 1–5, doi: 10.1109/CONIT59222.2023.10205634.

[7] R. Yang, C. Zhang, and Y. Cheng, "Real Time Continuous Image Stitching Algorithm Based on SIFT," in *2024 3rd International Joint Conference on Information and Communication Engineering (JCICE)*, May 2024, pp. 168–171, doi: 10.1109/JCICE61382.2024.00042.

[8] K. Su, "Underwater Image Stitching Algorithm Based on RANSAC+SIFT," in *2023 5th International Conference on Frontiers Technology of Information and Computer (ICFTIC)*, Nov. 2023, pp. 525–528, doi: 10.1109/ICFTIC59930.2023.10456346.

[9] A. R. Al-Shamasneh, "Automatic Enlarged Lymph Node Detection by Volume Estimation from 3D Abdominal CT Images Based on Speed Up Robust Features and Maximum Intensity Projection," in *2023 International Conference on Smart Computing and Application (ICSCA)*, Feb. 2023, pp. 1–6, doi: 10.1109/ICSCA57840.2023.10087456.

[10] I. Yuadi, U. Nihaya, F. D. Pratiwi, and A. T. Asyhari, "Book Spine Matching with Library Collection Using Speeded Up Robust Features," in *2023 8th International Conference on Electrical, Electronics and Information Engineering (ICEEIE)*, Sep. 2023, pp. 1–5, doi: 10.1109/ICEEIE59078.2023.10334671.

[11] A. Kashyap, B. Suresh, and K. D. Tyagi, "Detection of Counterfeit Currency Through SURF and Haar Cascade Classifier," in *2023 9th International Conference on Signal Processing and Communication (ICSC)*, Dec. 2023, pp. 296–301, doi: 10.1109/ICSC60394.2023.10441382.

[12] A. R. Al-Shamasneh and N. Althuniyan, "Automatic Enlarged Lymph Node Detection from 3D Mediastinum CT Images," in *2023 Sixth International Conference of Women in Data Science at Prince Sultan University (WiDS PSU)*, Mar. 2023, pp. 47–52, doi: 10.1109/WiDS-PSU57071.2023.00022.

[13] L. Ouyang, R. Lu, Y. Ye, M. Xing, and Q. Cai, "Feature Point Extraction and Matching Based on Improved SURF Algorithm," in *2023 China Automation Congress (CAC)*, Nov. 2023, pp. 1846–1851, doi: 10.1109/CAC59555.2023.10450357.

[14] F. Yang and X. Ye, "Research on a Fast Image Stitching Method Based on Improved SURF Algorithm," in *2023 2nd International Conference on Artificial Intelligence and Computer Information Technology (AICIT)*, Sep. 2023, pp. 1–4, doi: 10.1109/AICIT59054.2023.10277768.

[15] X. Zhu, Z. Li, C. Sun, J. Chang, and W. Li, "Fast Aerial Image Stitching Algorithm for UAV Based on Improved SURF," in *2023 China Automation Congress (CAC)*, Nov. 2023, pp. 7598–7604, doi: 10.1109/CAC59555.2023.10450367.

[16] Y. Luo, "Research on Image Matching in Indoor Environments Based on Enhanced SURF and RANSAC Algorithms," in *2024 IEEE 6th International Conference on Civil Aviation Safety and Information Technology (ICCASIT)*, Oct. 2024, pp. 143–148, doi: 10.1109/ICCASIT62299.2024.10828043.

[17] J. Yu, D. Huang, J. Li, W. Li, X. Wang, and X. Shi, "Parallel Acceleration of Real-time Feature Extraction Based on SURF Algorithm," in *2023 15th International Conference on Computer Research and Development (ICCRD)*, Jan. 2023, pp. 57–63, doi: 10.1109/ICCRD56364.2023.10079983.

[18] J. Hao, J. Xie, J. Zhang, and M. Liu, "A Stronger Stitching Algorithm for Fisheye Images Based on Deblurring and Registration," *IEEE Sensors Lett.*, vol. 7, no. 10, pp. 1–4, Oct. 2023, doi: 10.1109/LSENS.2023.3320060.

[19] P. H. S. Torr and A. Zisserman, "MLESAC: A New Robust Estimator with Application to Estimating Image Geometry," *Comput. Vis. Image Underst.*, vol. 78, no. 1, pp. 138–156, Apr. 2000, doi: 10.1006/cviu.1999.0832.

[20] Y. Mo, X. Kang, P. Duan, and S. Li, "A Robust UAV Hyperspectral Image Stitching Method Based on Deep Feature Matching," *IEEE Trans. Geosci. Remote Sens.*, vol. 60, pp. 1–14, 2022, doi: 10.1109/TGRS.2021.3123980.

[21] H.-I. Lin, M. Ahsan Fatwaddin Shodiq, A.-K. Jeng, and C.-W. Chang, "An Efficient Large-Scale 3D Map Stitching Algorithm Using Automatic Overlapping Area Identification," *IEEE Access*, vol. 13, pp. 42587–42607, 2025, doi: 10.1109/ACCESS.2025.3548859.

[22] F. Wu, K. Tan, X. Wang, J. Ding, and Z. Liu, "A novel semi-empirical soil multi-factor radiative transfer model for soil organic matter estimation based on hyperspectral imagery," *Geoderma*, vol. 437, p. 116605, Sep. 2023, doi: 10.1016/j.geoderma.2023.116605.

[23] F. Dai and S. Gao, "Optimal Design of a PIDD 2 Controller for an AVR System Using Hybrid Whale Optimization Algorithm," *IEEE Access*, vol. 12, pp. 128525–128540, 2024, doi: 10.1109/ACCESS.2024.3454107.

[24] A. Ardiansyah, M. I. Zulfa, A. Tarmuji, and F. H. Jabbar, "Optimization of use case point through the use of metaheuristic algorithm in estimating software effort," *Int. J. Adv. Intell. Informatics*, vol. 10, no. 1, p. 109, Feb. 2024, doi: 10.26555/ijain.v10i1.1298.

[25] Y. Zheng, C. J. You, N. Zhang, X. Zhu, Y. Ding, and H. He, "Wide-Angle Scanning Thinned Phased Array Synthesis Based on Improved Multiobjective Beluga Whale Optimization Algorithm," *IEEE Antennas Wirel. Propag. Lett.*, vol. 23, no. 11, pp. 3511–3515, Nov. 2024, doi: 10.1109/LAWP.2024.3416174.

[26] Y. Li, Z. Xie, S. Yang, and Z. Ren, "A Novel Hybrid Multi-Objective Optimization Algorithm and Its Application to Designs of Electromagnetic Devices," *IEEE Trans. Magn.*, vol. 61, no. 2, pp. 1–4, Feb. 2025, doi: 10.1109/TMAG.2024.3519202.

[27] K. Nuaekaew, P. Artrit, N. Pholdee, and S. Bureerat, "Optimal reactive power dispatch problem using a two-archive multi-objective grey wolf optimizer," *Expert Syst. Appl.*, vol. 87, pp. 79–89, Nov. 2017, doi: 10.1016/j.eswa.2017.06.009.

[28] X. Chen, M. Ma, C. Liu, H. Xie, and S. Wang, "Research on Interference Resource Optimization Based on Improved Whale Optimization Algorithm," *IEEE Access*, vol. 13, pp. 83136–83147, 2025, doi: 10.1109/ACCESS.2025.3569460.

[29] C. Li, C. You, Y. Gu, and Y. Zhu, "Parameter Identification of the RBF-ARX Model Based on the Hybrid Whale Optimization Algorithm," *IEEE Trans. Circuits Syst. II Express Briefs*, vol. 71, no. 5, pp. 2774–2778, May 2024, doi: 10.1109/TCSII.2024.3351848.

[30] Z. Lu *et al.*, "Inversion of Bubble Size Distribution Based on Whale Optimization Algorithm," *IEEE Photonics J.*, vol. 16, no. 4, pp. 1–6, Aug. 2024, doi: 10.1109/JPHOT.2024.3406886.

[31] H. P. Hsu and C. N. Wang, "Hybridizing Whale Optimization Algorithm With Particle Swarm Optimization for Scheduling a Dual-Command Storage/Retrieval Machine," *IEEE Access*, vol. 11, pp. 21264–21282, 2023, doi: 10.1109/ACCESS.2023.3246518.

[32] S. Yin, J. Yang, L. Ma, M. Fu, and K. Xu, "An Enhanced Whale Algorithm for Three-Dimensional Path Planning for Meteorological Detection of the Unmanned Aerial Vehicle in Complex Environments," *IEEE Access*, vol. 12, pp. 60039–60057, 2024, doi: 10.1109/ACCESS.2024.3394055.

[33] Z. H. Zhao, Y. F. Yin, Y. K. Wang, K. R. Qin, and C. D. Xue, "Adaptive ECG Signal Denoising Algorithm Based on the Improved Whale Optimization Algorithm," *IEEE Sens. J.*, vol. 24, no. 21, pp. 34788–34797, 2024, doi: 10.1109/JSEN.2024.3422995.

[34] R. Chatterjee *et al.*, "FNN for Diabetic Prediction Using Oppositional Whale Optimization Algorithm," *IEEE Access*, vol. 12, pp. 20396–20408, 2024, doi: 10.1109/ACCESS.2024.3357993.

[35] X. Yang and J. Guan, "PI Parameters Tuning for Frequency Tracking Control of Wireless Power Transfer System Based on Improved Whale Optimization Algorithm," *IEEE Access*, vol. 12, pp. 13055–13069, 2024, doi: 10.1109/ACCESS.2024.3355965.

[36] H. Wu, S. Du, Y. Zhang, Q. Zhang, K. Duan, and Y. Lin, "Threshold Binary Grey Wolf Optimizer Based on Multi-Elite Interaction for Feature Selection," *IEEE Access*, vol. 11, pp. 34332–34348, 2023, doi: 10.1109/ACCESS.2023.3263584.

[37] F. A. Saif, R. Latip, Z. M. Hanapi, and K. Shafinah, "Multi-Objective Grey Wolf Optimizer Algorithm for Task Scheduling in Cloud-Fog Computing," *IEEE Access*, vol. 11, pp. 20635–20646, 2023, doi: 10.1109/ACCESS.2023.3241240.

[38] W. Liu, Z. Ding, H. Zhang, and M. Zhu, "Multiobjective Optimal Power Flow for Distribution Networks Utilizing a Novel Heuristic Algorithm—Grey Wolf Equilibrium Optimizer," *IEEE Syst. J.*, vol. 18, no. 1, pp. 174–185, Mar. 2024, doi: 10.1109/JSYST.2024.3352235.

[39] A. Toktas, U. Erkan, D. Ustun, and Q. Lai, "Multiobjective Design of 2D Hyperchaotic System Using Leader Pareto Grey Wolf Optimizer," *IEEE Trans. Syst. Man, Cybern. Syst.*, vol. 54, no. 9, pp. 5237–5247, Sep. 2024, doi: 10.1109/TSMC.2024.3401412.

[40] Q. Zhang, J. Zhao, L. Pan, X. Wu, Y. Hou, and X. Qi, "Optimal Path Planning for Mobile Robots in Complex Environments Based on the Gray Wolf Algorithm and Self-Powered Sensors," *IEEE Sens. J.*, vol. 23, no. 18, pp. 20756–20765, Sep. 2023, doi: 10.1109/JSEN.2023.3252635.

[41] C. Sun, H. Sang, L. Meng, B. Zhang, and T. Meng, "Efficient Multi-Start Gray Wolf Optimization Algorithm for the Distributed Permutation Flowshop Scheduling Problem with Preventive Maintenance," *Complex Syst. Model. Simul.*, vol. 5, no. 2, pp. 107–124, Jun. 2025, doi: 10.23919/CSMS.2025.0001.

[42] L. Huang *et al.*, "Design Optimization of an Iron Core for Cup-Type AMF Contacts Using Genetic Aggregation Response Surface and Multi-Objective Genetic Algorithm," *IEEE Trans. Appl. Supercond.*, vol. 34, no. 8, pp. 1–5, Nov. 2024, doi: 10.1109/TASC.2024.3425352.

[43] L. Xing, Y. Wang, M. Li, N. Cheng, and H. Wu, "Multi-Objective Optimization Model of Electric Power Fine Construction Based on Multi-Objective Genetic Algorithm," in *2023 International Conference on*

Mechatronics, IoT and Industrial Informatics (ICMIII), Jun. 2023, pp. 576–581, doi: 10.1109/ICMIII58949.2023.00121.

[44] C. Liao, S. Wang, Z. Wang, and Y. Zhai, "GAA-DFQ: A Dual-Layer Learning Model for Robot Path Planning in Dynamic Environments Integrating Genetic Algorithms, DWA, Fuzzy Control and Q-Learning," in *2025 8th International Conference on Advanced Algorithms and Control Engineering (ICAACE)*, Mar. 2025, pp. 339–343, doi: 10.1109/ICAACE65325.2025.11019886.

[45] I. Naouadir, J. El Mekkaoui, A. Hjouji, O. El Ogri, and M. Benslimane, "Adaptive Genetic Algorithm for 2D Problems With a Dynamic Gene Walk," in *2024 3rd International Conference on Embedded Systems and Artificial Intelligence (ESAI)*, Dec. 2024, pp. 1–6, doi: 10.1109/ESAI62891.2024.10913704.

[46] K. Chen, C. Peng, S. Shi, Y. Zhang, X. Zhang, and F. Zhang, "Multi-Objective collaborative research on green construction of power grid projects based on genetic algorithms," in *2024 5th International Conference on Artificial Intelligence and Electromechanical Automation (AIEA)*, Jun. 2024, pp. 479–484, doi: 10.1109/AIEA62095.2024.10692849.

[47] Y. Li, Z. Xie, S. Yang, and Z. Ren, "A Hybrid Algorithm Based on NSGA-II and MOPSO for Multi-Objective Designs of Electromagnetic Devices," *IEEE Trans. Magn.*, vol. 59, no. 5, pp. 1–4, May 2023, doi: 10.1109/TMAG.2023.3250319.

[48] X. Tan, T. Chen, H. Liu, S. Huang, Z. Zhuang, and Y. Hu, "A Multi-Objective Optimization Model for Electric Vehicle Scheduling under Charging Station Constraints," in *2024 2nd Power Electronics and Power System Conference (PEPSC)*, Nov. 2024, pp. 218–222, doi: 10.1109/PEPSC63375.2024.10823631.

[49] S. Liu, X. Li, and J. Hu, "Multi-UAV Path Planning for Multi-Region Coverage by Multi-Objective Genetic Method," in *2024 6th International Conference on Electronic Engineering and Informatics (EEI)*, Jun. 2024, pp. 1357–1362, doi: 10.1109/EEI63073.2024.10696389.

[50] A. Assistant Professor, "International Journal of Emerging Technologies in Computational and Applied Sciences(IJETCAS) www.iasir.net Image Mosaicking with Modified SURF," 2013. [Online]. Available at : https://iasir.net/files/ijetcaspapers/ijetcas13-182.pdf